HHS Public Access

Author manuscript

Ultrasound Med Biol. Author manuscript; available in PMC 2016 February 01.

Published in final edited form as:

Ultrasound Med Biol. 2015 February ; 41(2): 432–448. doi:10.1016/j.ultrasmedbio.2014.09.009.

Electrophysiological Changes Correlated with Temperature Increases Induced by High-Intensity Focused Ultrasound Ablation

Z. Wu[*], **R. E. Kumon**[*,&], **J. I. Laughner**[†], **I. R. Efimov**[†], and **C. X. Deng**[*]

[*]Department of Biomedical Engineering, University of Michigan, Ann Arbor, MI, USA

[†]Department of Biomedical Engineering, Washington University at Saint Louis, MO, USA

Abstract

To gain better understanding of the detailed mechanisms of high-intensity focused ultrasound (HIFU) ablation for cardiac arrhythmias, we investigated how the cellular electrophysiological (EP) changes were correlated with temperature increases and thermal dose (cumulative equivalent minutes [CEM_{43}]) during HIFU application using Langendorff-perfused rabbit hearts. Employing voltage-sensitive dye di-4-ANEPPS, we measured the EP and temperature during HIFU using simultaneous optical mapping and infrared imaging. Both action potential amplitude (APA) and AP duration at 50% repolarization (APD_{50}) decreased with temperature increases, and APD_{50} was more thermally sensitive than APA. EP and tissue changes were irreversible when HIFU-induced temperature increased above 52.3 ± 1.4 °C and $\log_{10}(CEM_{43})$ above 2.16 ± 0.51 (n = 5), but were reversible when temperature was below 50.1 ± 0.8 °C and $\log_{10}(CEM_{43})$ below −0.9 ± 0.3 (n = 9). EP and temperature/thermal dose changes were spatially correlated with HIFU induced tissue necrosis surrounded by a transition zone.

Keywords

Bioeffects; Langendorff-perfused rabbit hearts; High-intensity focused ultrasound; optical mapping; infrared imaging; cellular electrophysiology

Introduction

Cardiac arrhythmias are the irregular electrical activities during heart cycles. They greatly compromise the heart function and represent a major clinical problem affecting millions of patients (Kannel et al. 1987). Ablation therapy, including radiofrequency (RF), cryothermal, microwave, and laser ablation (Aktas et al. 2008; Dewire and Calkins 2010; Lall and

Corresponding Author: Cheri X. Deng, Department of Biomedical Engineering, University of Michigan, 2200 Bonisteel Blvd, Ann Arbor, MI 48109-2099, USA. Tel: +1 734-936-2855; Fax: +1 734-936-1905. cxdeng@umich.edu (C. X. Deng).

[&]Current address: Department of Physics, Kettering University, Flint, MI, USA

Damiano 2007; Scheinman and Morady 2001), has developed as an important treatment option. However, these ablation techniques require direct tissue contact and rely on thermal conduction, thus ablation depth is often limited and ablation volumes are not well-confined, leading to collateral damages (Lall and Damiano 2007) and unsuccessful outcomes (Nanthakumar et al. 2004).

High intensity focused ultrasound (HIFU) ablation uses concentrated ultrasound energy to generate rapid temperature increases and tissue modifications (e.g. protein denaturation and tissue coagulation) in a well-confined volume, without relying on heat conduction from tissue surface through intervening tissue. It provides a promising technology for cardiac ablation especially when intramural ablation is desired (Okumura et al. 2008). For example, HIFU has been used for atrio-ventricular node ablation (Strickberger et al. 1999) and pulmonary vein isolation (PVI) to treat paroxysmal atrial fibrillation (AF) in multicenter trials (Aktas et al. 2008; Ninet et al. 2005). One study reported that 85% of 103 patients treated with HIFU were free from AF at six-month follow-up (Aktas et al. 2008; Ninet et al. 2005). However, recent clinical trials using a HIFU balloon system (Neven et al. 2010) showed ablation-related complications including atrial-esophageal fistula, pulmonary embolism, and phrenic nerve injury, and 28% of 32 patients showed electrical reconduction after initial PVI and underwent repeated procedures (Metzner et al. 2010). These results indicate the need to better understand the detailed effects of HIFU in cardiac ablation to improve the technology.

As in other HIFU thermal applications, *in vitro* studies have investigated the relationships between HIFU conditions (e.g. acoustic power and exposure time) and tissue status changes (Engel et al. 2006; Fujikura et al. 2006; Zimmer et al. 1995), while temperature and thermal dose were often used as feedbacks in HIFU ablation and prediction of lesion formation (Rivens et al. 2007). It has been found that when tissue temperature reaches 50 °C or higher for certain duration, tissue necrosis occurs and becomes non-conductive (Haines 1993). In particular, changes in the cellular conductivity and excitability are important in cardiac ablation and the electrophysiological (EP) changes need to be monitored and ultimately confirmed to ensure successful isolation/elimination of arrhythmic foci. However, detailed spatiotemporal EP changes and their correlations with HIFU induced temperature or thermal dose increases have not been specifically investigated previously.

As the fundamental functional units, myocytes and their couplings are able to generate an electrical transient, the action potential (AP), while the initiation (depolarization) and termination (repolarization) of APs as well as their propagations among myocytes can affect the electrical functions of the whole heart (Giridhar et al. 2012). A few features such as resting membrane potentials (RMPs), AP amplitude (APA), AP duration (APD), and etc. (Nath et al. 1993; Wood and Fuller 2002; Wu et al. 1999) are often used to characterize AP morphology and the functionalities of myocytes. Nath *et al.* first demonstrated the EP properties as well as cellular automaticity and excitability were temperature dependent in hyperthermia (Nath et al. 1993), providing useful information for the development of RF and microwave ablation techniques. Haines (Haines 1993) and Wu *et al*. (Wu et al. 1999) further illustrated that RF energy had a combined thermal and electronic effect on changing cellular EP. Wood *et al*. later demonstrated that RF can induce acute cellular EP changes

surrounding RF lesions which can recover completely (Wood and Fuller 2002). Recently, three potential effects in HIFU cardiac ablation were identified including thermal, radiation force, and cavitation, and the latter two factors can interfere with HIFU thermal effect and lead to unsuccessful ablation (Laughner et al. 2012b). As the predominant mechanism of HIFU ablation was assumed to be thermal (Khokhlova et al. 2013), it is of interest to investigate whether HIFU cardiac ablation induce similar EP changes as in RF ablation and how HIFU induced lesions are correlated with cellular EP changes. Such information has not been available before but can reveal the detailed characteristics and mechanisms of HIFU ablation of cardiac arrhythmias and possibly other thermal ablation therapies.

Previously, we have demonstrated the feasibility of fluorescence optical mapping (Deng et al. 2005) for measuring HIFU-induced cardiac EP changes using Langendorff-perfused intact rabbit heart preparations. In the current study, by combining optical mapping with infrared (IR) thermography, we obtained the first simultaneous measurements of EP changes and temperature increases as well as thermal dose during HIFU application to help reveal their detailed spatiotemporal correlation in HIFU cardiac ablation.

Methods

Isolated Heart Preparations

New Zealand white rabbits (n = 11, ~ 3 kg) were used in the study according to a protocol approved by the Committee on the Use and Care of Animals at University of Michigan (Protocol #: PRO00003842). The animals were anesthetized intramuscularly via ketamine (35 mg/kg) and xylazine (5 mg/kg), heparinized (1000 U/kg), and euthanized intravenously by injection of sodium pentobarbital (100 mg/kg). The heart was harvested after mid-sternotomy, and rapidly washed with warmed Tyrode's solution. As described before (Laughner et al. 2012b), the heart was immediately placed on a Langendorff apparatus and retrogradely perfused with oxygenated Tyrode's solution (pH = 7.35 ± 0.05; 37 °C; 95% O_2/5% CO_2) via aorta at constant pressure (60 – 80 mmHg). Peripheral tissue was cleaned and the heart was superfused in Tyrode's solution at 35 – 37 °C. Excitation-contraction decoupler, 2, 3-butanedione monoxime (BDM, 15 mM; Fisher Scientific) was administered to mechanically silence the heart beat motion that can introduce artifacts during imaging. The electrocardiogram was recorded with two needle electrodes and digitized (Powerlab 26T, ADInstruments) while the aortic perfusion pressure was continuously monitored (BLPR2, World Precision Instruments) to ensure physiological stability of the heart preparation.

Experimental Setup with Simultaneous Optical Mapping and Infrared Imaging

As shown in Fig. 1, the heart preparation was placed in a custom-made holder with an acoustically transparent window (4.5 × 4.5 cm^2) for ultrasound transmission from below. The heart was pinned to a silicone gel pad (Sylgard 184, Dow Corning) in the holder, which was controlled using a 3D positioning stage (EPS300, Newport) for precise (50 μm) spatial alignment.

A concave single element HIFU transducer (2.0 MHz, H-148, Sonic Concepts) (focal length 63.2 mm and F-number 0.95), driven by a signal generator (33250A, Agilent) and a 75W power amplifier (75A250, Amplifier Research), was used to generate HIFU exposures. The focal peak compressional/rarefactional pressures were measured to be p_c = 7.0 – 8.7 MPa and p_r = −4.4 – −5.2 MPa in water (in free field) using a custom fiber optic probe hydrophone (FOPH) system (Parsons et al. 2006) with 6 % uncertainty (type B). The 6-dB focal zone was determined to be 7.2 × 0.9 mm (Length × Width) for p_c and 8.7 × 1.2 mm for p_r when I_{sppa} was at 846 W/cm^2. The corresponding spatial-peak pulse-average intensities (I_{sppa}) were calculated to be 846 – 1266 W/cm^2 using the equation (Zhou et al. 2006)

$$I_{sppa}=\frac{1}{nT}\int_{t_0}^{t_0+nT}\frac{p^2(t)}{\rho_0 c_0}dt \quad (1)$$

where $p(t)$ is the transient pressure value at time t; ρ_0 and c_0 are the density and speed of sound of the ambient water, respectively; t_0 is the starting time of a full pressure waveform; nT is integer periods of pressure waveforms whereas t is the time. A power meter (PM-1, JJ&A Instruments) was inserted to monitor electrical power output and to ensure stable power output as well as detect impedance mismatch between amplifier and HIFU transducer. The transducer was fixed at the bottom of the tank, facing upward with its focus (maximum peak positive pressure) placed on the epicardium of either right or left ventricle of the heart preparation through the acoustic window (Fig. 1A). The HIFU focus was positioned at the targeted region by employing a pulse/echo method that detected the location of epicardium/air interface based on the time of flight of the echoes. Considering acoustic attenuation (~ 2 dB/cm·MHz in heart tissue (Azhari 2010)) and an acoustic travelling distance in the heart tissue (~ 1cm), the *in situ* pressures for a traveling wave would be p_c = 4.4 – 5.5 MPa and p_r = −2.8 – −3.3 MPa at the HIFU focus. Since the heart was placed sideways with one side of the heart surface slightly above the solution to allow IR imaging, the tissue/air interface in our experimental setup may result in reflection of the HIFU beam and affected the actual pressure field *in situ*. Thus we estimated that the *in situ* I_{sppa} were 1344 – 2010 W/cm^2.

The isolated heart was perfused and stained with a voltage-sensitive dye (VSD) di-4-ANEPPS (Invitrogen) (10 μM) for 10 – 15 mins before optical mapping. The particular VSD are amphipathic molecules, which can bond to the membranes of myocytes and become fluorescent whereas the fluorescent intensities are proportional to the membrane potentials (Loew 1992). Because of their fast response to the changes of ambient electrical field, the APs of myocytes can be recorded via optical mapping, which used two green-filtered light-emitting diodes (5G Illumination system, SciMedia USA) for excitation (~531 nm) and corresponding emission. Fluorescence signals were filtered (> 617 nm) and recorded using a CMOS camera system (MiCAM Ultima-L, SciMedia USA) at 1000 frames/s with a spatial resolution of 420 – 460 μm/pixel (100 × 100 pixels). Since the recorded optical signals are weighted summation of emitted fluorescence from cells within a tissue depth less than 200 μm below the surface for rabbit hearts due to tissue absorption and photonic scattering (Knisley 1995), optical mapping measures the EP of cells in a superficial layer.

The upper surface of the heart preparation was elevated slightly above the solution to allow IR imaging. The IR camera (Silver SC5600, FLIR) was confocally aligned with the CMOS camera to measure temperature at 50 frames/s and with a focal resolution of 85 μm in the same region of interest (ROI) on the epicardium (Fig. 1B) with optical mapping (Fig. 1C). The emissivity of the heart tissue was calibrated to be 0.86 prior to experiments using a black tape method (Madding 1999) which used a vinyl electrical tape (Scotch Super33+, 3M) with a known emissivity of 0.95. Because of the temperature difference between the perfusate within the heart (37 °C) and air (23 °C), 2 °C temperature loss due to heat convection was observed and the baseline temperature of the heart was measured as 35 °C by IR imaging (Fig. 2B). However, no temperature compensation (e.g. constant +2 °C) was performed on IR imaging data as it might be inaccurate during HIFU heating process.

The CMOS and IR cameras were synchronized with HIFU via a FPGA board (Cyclone® II, Altera) to recode optical action potentials (OAPs) and surface temperature of the isolated heart during HIFU application.

Experimental Procedure

During experiment, the Langendorff-perfused rabbit heart was under its natural rhythm (sinus rhythm). To maximize the signal-noise-ratio for optical mapping, the excitation light was adjusted following 10 – 15 min equilibration, by setting the highest pixel intensity slightly higher than 80% of the saturation level over several cardiac cycles. Ten seconds tone-burst HIFU with *in situ* intensity varying from 1344 to 2010 W/cm^2 was applied to the heart preparation. Such intensities were high enough to ensure lesion generation or EP changes while sufficiently low to avoid lifting epicardium out of the focus of optical mapping and IR imaging due to acoustic radiation force. After experiment, the heart was photographed (D5000, Nikon), stained with triphenyltetrazolium (TTC) (Sigma Aldrich) (Fishbein et al. 1981) where necrotic tissue was stained as white and viable tissue was in dark red. Gross tissue was then stored in 10% formalin solution for 48 hours, paraffin embedded, and sectioned at 100 μm step size across the region along the transmural direction. Masson's trichrome (MT) staining was conducted on tissue sections and the stained slides were scanned with high resolution (CanoScan 8800F, Canon). HIFU-induced lesions were then identified from the images.

Image Processing and Data Analysis

IR images were scaled to the size of VSD images via bilinear interpolation. Each pair of optical-IR images was registered using a control point registration algorithm (Matlab v. 2011b, Mathworks) (Figs. 1B – E). Multiple common identifiable feature points (8 to 10) on both images were picked and a projective transformation was performed to compensate the error induced by the angle differences between the two cameras.

Spatial averaging (3 × 3) and a zero-phase band-pass (0 – 100 Hz) filter were applied for spatiotemporal smoothing of the VSD images (Laughner et al. 2012a). The effects of photo bleaching were corrected using exponential, 2nd order polynomial, and linear fitting of the VSD baseline values prior, during, and after HIFU application respectively. OAPs were normalized from 0 to unity and AP amplitude (APA) was defined as the value between

OAPs peaks and resting potentials. Activation time was identified as the corresponding times when d(Δ*F*)/dt reached maximum within an individual cardiac cycle, where Δ*F*, or fractional fluorescence change, was the ratio between change of fluorescence signal intensity and the background fluorescence level. Activation maps were formed from the activation time at each pixel and conduction velocities (CVs) were derived as the spatial gradient of the activation map. AP duration at 50% repolarization (APD_{50}) was defined as the duration between activation time and 50% peak APA value at repolarization. Changes in APA (ΔAPA), APD_{50} (ΔAPD_{50}), and activation times (Δactivation) were calculated by subtracting the pre-HIFU baseline values.

To evaluate the HIFU energy deposition, thermal dose or specifically the cumulative equivalent minutes at 43 °C (denoted as CEM_{43}) (Sapareto and Dewey 1984) was calculated as

$$CEM_{43} = \sum_{t=0}^{t_{final}} R^{(43-\overline{T})} \Delta t \quad (2)$$

where $\overline{T}$ is the average temperature during time duration Δ*t*, t_{final} is the final time of exposure, $R = 0.25$ when the temperature is below 43 °C and $R = 0.5$ when the temperature is above 43 °C.

The HIFU lesion, as identified from images of TTC stained tissue specimens, was denoted as positive whereas non-lesion region was denoted as negative. Receiver-operating characteristic (ROC) analysis was performed on temperature and EP maps at $t = 14$ s (HIFU application was from 4 to 14 s) and CEM_{43} maps at $t = 32$ s to predict isotherms of lesion, APA changes, and APD_{50} changes. ROC curves were formed by comparing true positive rate (sensitivity) against false positive rate (1 – specificity) at all running thresholds and total area under curve (AUC) was used to assess the overall prediction performance. The optimal temperature threshold for generating lesion (lethal isotherm) was decided based on the best detection accuracy. Leave-one-out cross-validation was used to determine the variation of ROC AUC and optimal temperature thresholds.

Results were expressed as mean ± standard error of mean (SEM). One-way analysis-of-variance (ANOVA) using the Tukey-Kramer test and paired Student-*t* test were performed for multiple group comparisons, with statistical significance defined as $p < 0.05$. Linear regression and *F*-test were conducted for testing linear correlation between parameters, and goodness-of-fit was assessed by the adjusted R^2 and root mean square error (*RMSE*) of the residuals.

Results

Spatiotemporally Correlated IR Imaging and Optical Mapping

Figures 1B – E show an example of spatiotemporally registered IR imaging and optical mapping during HIFU ablation of the heart preparations. The IR image (Fig. 1C) was

projective transformed and registered with the VSD image (Fig. 1D). Figure 1E shows a composite image with IR image overlaid on the VSD image for ROI analysis.

Effect of HIFU on the OAPs Baseline

During HIFU ablation, IR imaging captured the spatiotemporal changes of tissue temperature (Figs. 2A – B), while a baseline drift of OAPs (thick line, Fig. 2C) appeared to be proportional to the temperature increases. The 2D maps of OAPs baseline (ΔB) within a ROI (17 × 17 pixels) surrounding the HIFU focus and the corresponding temperature changes (ΔT) were spatiotemporally correlated, especially during HIFU application (4 s – 14 s) (Fig. 2D). The ratiometric maps ($\Delta B/\Delta T$) (bottom row in Fig. 2D) at given times were fairly uniform within the ROI when ΔT was greater than 5 °C, indicating a linear correlation between ΔB and ΔT in 2D space. Such linear correlation was confirmed through *F*-test, and the overall linear regression slope during HIFU heating was $(29.91 \pm 0.09) \times 10^{-2}$ %/°C (adj. $R^2 = 0.78$, 16 frames × 7 heart preparations) with *RMSE* being 0.27 %. However, linear regressions between ΔB and ΔT varied temporally (Fig. 2E) with the regression slope values increasing during HIFU application, especially at the beginning of HIFU exposure, suggesting a slow response of the baseline ΔB changes when ΔT was increasing. The ΔB–ΔT correlation was better during HIFU application (adj. $R^2 = 0.75 \pm 0.04$) than during post-HIFU cooling period (adj. $R^2 < 0.5$) (Fig. 2E) with smaller variations during heating (< 0.03 %/°C) than during cooling (> 0.05 %/°C).

HIFU induced spatiotemporal EP and Temperature Changes

Two dimensional characteristics of cardiac EP including APA, APD, and AP triangulation (APD_{50}/APD_{80}) were quantified and spatiotemporally correlated with temperature/thermal dose changes during HIFU application, and temperature/thermal dose-dependent AP changes were derived in the end.

(1) Reversible EP Changes—At HIFU intensities I_{sppa} = 1344 – 1660 W/cm^2 and 10 s exposure, no tissue necrosis was observed in the heart preparations ($n = 9$) (Fig. 3A) while the peak temperature was below 50.1 ± 0.8 °C (45.0 ~ 56.6 °C) ($n = 9$) (Fig. 3D) and CEM_{43} was less than 6.0 mins ($\log_{10}(CEM_{43}) = -0.9 \pm 0.3$). HIFU has generated morphological changes on OAPs including AP amplitude reduction and shortening of AP duration (Figs. 3B – C). After cessation of HIFU, the OAPs recovered instantaneously and the recovery was almost complete (to > 95% of the pre-HIFU level). Temperature was the highest at the HIFU focus, and its amplitude decreased radially at locations further away from the focus (Fig. 3D). A slight asymmetric temperature distribution around the HIFU focus was sometimes observed, likely due to heterogeneous myocardial fiber orientation and microvasculature perfusion.

Corresponding to the radially decreased temperature distribution, spatial distribution of APA and APD_{50} reductions were observed surrounding the HIFU focus (Figs. 3E – F). Notably, the region of APA reduction was more localized than that of APD_{50} reduction. In addition, APA reduction outpaced APD_{50} reduction during HIFU application (Fig. 3G), and no significant disproportional APD changes ($\Delta APD_{50}/\Delta APD_{80}$) were observed (Fig. 3H), suggesting negligible AP triangulation and loss of plateau potentials in these cases. For

smaller temperature increases less than 50.1 ± 0.8 °C and CEM_{43} less than 6.0 mins, APA and APD changes along with activation distortion were reversible without tissue necrosis presented on MT stained histological slides; whereas the APA and activation changes appear to recover faster than APD_{50}, suggesting a slower response for APD changes comparing with APA changes.

Furthermore, the activation isochrones were clustered when electrical wavefronts propagated across the HIFU focal region: the activation time was delayed by up to 5 ms, and CV increased by ~ 1.3 mm/ms within and surrounding the HIFU focus respectively (Figs. 4A1 – C1).

(2) Irreversible EP Changes—At a higher HIFU intensity (e.g. I_{sppa} = 2010 W/cm^2), tissue necrosis or thermal lesions (Fig. 5A) were generated by HIFU application. Lesions were generally elliptical along the depth direction and circular in lateral direction, and the transmural cross-section areas were 5.95 ± 0.99 mm^2, with axial depths of 3.55 ± 0.38 mm and lateral widths of 2.10 ± 0.14 mm (n = 6). APA and APD_{50} reduced by 32% and 52 ms respectively, as illustrated by the OAPs at representative locations in the HIFU focus (lesion) and surrounding tissue region (control) (Figs. 5B – C). Significant APD reduction and triangulation of OAPs morphology were observed (Fig. 5C) compared to the cases showing reversible EP changes without tissue necrosis (Fig. 3), indicating that plateau potentials of OAPs were significantly suppressed by HIFU ablation at higher intensity. After HIFU ablation (Fig. 5C, t = 31 s), APA recovered partially to only 73% of the pre-HIFU values, suggesting an irreversible loss of cellular excitability.

Compared to the reversible cases, increased HIFU intensity generated higher temperature increases in tissue where the peak temperature reached 66.4 ± 8.5 °C (52.1 ~ 84.9 °C) (Fig. 5D) and peak CEM_{43} at t = 32 s was greater than 234.4 mins ($\log_{10}(CEM_{43})$ = 4.2 ± 1.8). Steeper temperature gradients were seen compared with previous cases (Fig. 3), along with similar spatial distribution of temperature increases around the HIFU focus (Fig. 5D).

Unlike the reversible cases, the corresponding OAPs showed sustained changes of APA and APD_{50} after the cessation of HIFU (Figs. 5E – F). A more significant activation isochronal clustering and changes of CVs were seen as the electrical wave propagated across the lesion area (Figs. 4A2 – C2) where a typical activation delay “tail” often seen in single spot ablation was easily identified (Fig. 4C2). Local activation delay recovered slightly due to phone scattering from the peripheral recovered tissue. Similar to the reversible cases, the areas with APA changes were smaller than the areas with APD_{50} changes, while certain regions underwent only APD changes, suggesting a higher thermal sensitivity for APDs, which are affected by both cell-cell coupling and ion channels dynamics in AP plateau phase (Figs. 5E – F). This is consistent with previously reported result that APD_{50} has a lower thermal threshold (Nath et al. 1993). Different from the reversible cases, however, the changes of APA outpaced ΔAPD_{50} from the beginning of HIFU application (Fig. 5G) and significant AP triangulation ($\Delta APD_{50}/\Delta APD_{80}$) occurred around the HIFU focus when lesions were generated (Fig. 5H).

Characteristics of EP Changes Corresponding to Temperature/Thermal Dose Changes

We categorized the HIFU ablation outcomes into two groups: the group with reversible EP change or damage (RD) (n = 9) without lesion formation (Fig. 3), and the group with irreversible EP damage (ID) (n = 6) and lesion formation (Fig. 5). The HIFU induced temperature and thermal dose increases in the ID group were significantly higher than those obtained in the RD group (Fig. 6A – B), with maximum temperatures (T_{max}) being 50.1 ± 0.8 °C vs. 66.4 ± 8.5 °C and CEM_{43} being below 6.0 mins vs. above 234.4 mins for the RD and ID, respectively. For both groups, ΔAPA and ΔAPD_{50} increased during HIFU heating (Figs. 6C – D). The APA eventually recovered after HIFU application for RD (− 0.05 ± 0.01) whereas continued to be irreversible for ID (− 0.27 ± 0.04) with significant difference ($p \ll 0.05$). However, ΔAPD_{50} were similar between both groups during HIFU heating, and their values after HIFU showed only slight difference (− 0.13 ± 0.02 vs. − 0.18 ± 0.03 for RD and ID respectively, $p \ll 0.05$), suggesting HIFU induced APA changes were a better discriminant feature for determining EP and tissue reversibility.

Figure 7 demonstrates the temporal correlation between EP parameters and HIFU induced temperature and thermal dose changes, where the values of ΔAPA and ΔAPD_{50} within the HIFU focus for RD, ID, and control (normal tissue outside HIFU focus) were plotted against the corresponding temperatures and thermal dose. During HIFU heating, the absolute values of ΔAPA increased with increasing temperature (Fig. 7A). The increase was slow at lower temperature, but as temperature reached above 51°C, larger ΔAPA were induced and became irreversible (ID group). Similar dependence on CEM_{43} was also seen (Fig. 7C), and faster and larger increases of ΔAPA occurred when $\log_{10}(CME_{43})$ was above −3.7. During post HIFU cooling (left arrows in Fig. 7A), ΔAPA recovered following the same trajectory as of HIFU heating with a fast initial recovery for the RD group, but continued to be irreversible for the ID group. APD_{50} however seemed to decrease linearly with the increasing temperature and CEM_{43} upon HIFU application (Fig. 7B and 7D). Compared with the APA dynamics which had a slower transition phase at the beginning, the instantaneity of APD_{50} reduction upon HIFU application suggests a lower thermal threshold for APD_{50} changes. The linear dependence of APD_{50} changes with temperature/CEM_{43} indicates that the dominant effect for HIFU ablation in altering cardiac EP is thermal (Wu et al. 1999). As APD_{50} recovered for both groups, significant hysteresis phenomena between heating and cooling paths was observed for ID group (Fig. 7B), indicating a severe irreversible damages on cellular AP due to HIFU application.

Spatial Characteristics of EP Changes Associated with Lesions

For both reversible and irreversible cases in this study, we observed that the region with APA changes were significantly smaller than the region with APD_{50} changes (Figs. 3 and 5). Profiles of temperature, CEM_{43}, and AP parameters along the diameter of the HIFU focus (Fig. 8A – B) confirmed that temperature/CEM_{43} decreased with increasing distance from the HIFU focus where ΔAPA and ΔAPD_{50} were the largest (Fig. 8A and 8B). Sharper spatial gradient of ΔAPA was seen as compared to the gradient of ΔAPD_{50}. Taking account of both EP and tissue physical changes, the HIFU ablated areas were characterized into three zones: *lesion zone* (e.g. $r < 1.05 \pm 0.07$ mm) where tissue necrosis was present with significant reduction on both APA and APD_{50}; *transition zone* (e.g. $r < 2.00 \pm 0.22$ mm)

with no lesion but with detectable reductions of APA and APD_{50}; and *remote zone* (e.g. $r <$ 3.79 ± 0.35 mm) where no tissue physical changes occurred but with apparent APD_{50} reduction. Within each zone, different pathological characteristics can be seen (Fig. 8C): in the lesion zone (Fig. 8C2), hyper-eosinophilic (H&E) stained cells, which indicate thermally induced protein denaturation were observed, and cellular structures were incomplete with deranged myofibrils and enlarged interstitial spaces; in the transition zone or lesion border zone (Fig. 8C3), an inflammatory rim with a narrow condensed necrotic band (50 – 70 μm) were apparent with mason's trichrome staining; in the remote zone (Fig. 8C4), cellular structure were intact without significant morphological changes.

By overlaying temperature and CEM_{43} maps on the binary masks derived from lesion image and at given EP thresholds, we determined isotherms of temperature and CEM_{43} for generating tissue necrosis, APA, and APD_{50} changes respectively using ROC analysis (Fig. 9, Table 1). The masks of ΔAPA and ΔAPD_{50} were generated using threshold values of −0.08 and −0.10, which were significantly above the background noise level (−0.05 ± 0.03 and −0.06 ± 0.04). The temperature isotherms were found to be 52.3 ± 1.4 °C, 42.2 ± 0.3 °C, and 39.1 ± 0.1 °C for generating lesions, ΔAPA, and ΔAPD_{50} respectively. Corresponding thresholds for $\log_{10}(CEM_{43})$ were 2.16 ± 0.51, −5.3 ± 0.13, and −6.73 ± 0.06. The isotherms for ΔAPD_{50} are lower than the isotherms for ΔAPA, suggesting APD_{50} is more thermally sensitive and the ion channels and pumps governing cellular plateau potentials have lower temperature thresholds than the ones provoking cellular action potentials.

Heat Conduction by Vessel Affected HIFU Ablation

Blood flow has been known to affect thermal ablation by acting as a "heat sink" which conducts heat away (Fuller and Wood 2003; Haines 1993). In this study, we investigated the effect of perfusion in HIFU ablation as well when the HIFU focus was near a lateral anterior descending (LAD) coronary artery (Fig. 10A, diagonal branch) and intensity was set at 2010 W/cm^2, same as that used for generating lesion. However, no tissue necrosis was generated in these experiments and reversible EP changes were observed instead ($n = 7$).

It was clearly shown on IR imaging that the heat was conducted away from the target zone by perfusion of the LAD coronary artery (the "tail" near the upper left of ablation zone [arrow] in Fig. 10B). The maximum temperature (T_{max}) achieved was less than 51.1 ± 1.4 °C ($n = 7$), significantly lower than the temperature obtained for the ID group (66.4 ± 8.5 °C). No tissue necrosis was detected, and changes of APA and APD_{50} were both transient (Figs. 10C – D).

Histological examination further illustrated the effect of vessel perfusion on HIFU ablation. Figures 10F – G show an example different from Figs. 10A – D with a LAD coronary artery in the center of the HIFU axial beam on a lesion specimen. After MT staining, viable cardiomyocytes were observed surrounding the LAD coronary artery possibly because of heat conduction by the artery during HIFU ablation. Compared with the case when LAD coronary artery was outside the HIFU beam (Fig. 10E), an asymmetric lesion along the HIFU beam was formed (Fig. 10F).

Discussion

We conducted spatiotemporally correlated optical mapping of cardiac EP and IR imaging of temperature and thermal dose during HIFU ablation to investigate how EP changes were affected by HIFU induced temperature changes and tissue necrosis. The major findings of this study are that (1) HIFU induced EP changes included temperature/thermal dose-dependent reduction of APA, shortening of APD, activation delay, and increases of conduction velocities around HIFU focus; (2) tissue EP changes were mostly reversible with temperature increases below 50.1 ± 0.8 °C and $\log_{10}(CEM_{43})$ less than − 0.9 ± 0.3; (3) irreversible EP changes along with tissue necrosis occurred as HIFU-induced temperature was above 52.3 ± 1.4 °C and $\log_{10}(CEM_{43})$ greater than 2.16 ± 0.51; (4) APD_{50} was more thermally sensitive than APA, and APA decreased nonlinearly whereas APD_{50} decreased linearly with temperature increases during HIFU application; (5) HIFU-ablated regions could be characterized into three zones with different tissue histological and EP properties; and (6) OAP baseline drifts were linearly correlated with HIFU induced temperature increases. We also showed the effect of vessel perfusion cooling on EP and temperature during HIFU ablation.

Spatiotemporal IR imaging and optical mapping

Direct temperature measurement traditionally relies on the use of thermocouples. However, insertion of thermocouples into tissue is not always convenient and feasible, particularly for HIFU ablation as they may interrupt the acoustic field. It is also potentially inaccurate to directly extrapolate one-dimensional temperature measures attained by thermistors at discrete locations into two-dimensional space (2D). The thermocouples themselves may introduce errors in temperature measurements by creating a “heat sink” effect via thermal conduction and “viscous heating” as well (Rivens et al. 2007). Several recent studies investigated infrared imaging as a novel tool to measure ultrasound field and beam intensities (Giridhar et al. 2012; Khokhlova et al. 2013). In this study, we employed IR thermometry allowing us directly measure the temperature changes in 2D space continuously in a noncontact fashion with high spatiotemporal (< 100 μm, 50 Hz) resolution that is not possible using individual thermistors (Fig. 1), and thermal dose information can be obtained by using the recorded temporal history of temperature. Moreover, due to spectrum similarity (infrared vs. near-infrared VSD emission), both IR imaging and optical mapping measure signals from the same tissue layers (e.g. epicardium and sub-epicardium, IR < 50 μm vs. optical mapping for 200 μm), therefore providing a well-suited combination to obtain temperature maps that can be spatiotemporally correlated with OAP signals. These measurements were obtained at the tissue surface and do not necessarily represent the effect of HIFU deep within the tissue. Nevertheless, it is expected that the EP changes in deep tissue be also correlated to the HIFU induced temperature increases there. In a recent study, by using an iterative finite-element method, Yin *et al.* successfully reconstructed the temperature changes induced by HIFU within the subsurface 3D volume using the spatiotemporal IR thermography (Knisley 1995).

The characteristics of epicardial EP could be different than EP within mid- and endocardium. For example, the APD_{50} is longest at endocardium but shortest at epicardium.

However, our previous work demonstrated that the changes of APD_{50} across the depth direction of myocardium during HIFU ablation were similar (Wu et al. 2013), suggesting the temperature-EP correlation derived from the surface measurement can still be applicable for subsurface condition. Nevertheless, the surface measurements in this study where the EP and temperatures were obtained from the same tissue layer can be correlated.

OAP Baseline Changes Measured during RF Ablation

Wu *et al.* observed the OAP baseline shifts during RF ablation (Wu et al. 1999), however the baseline changes can be prone to artifacts due to tissue-probe contact and movement of the RF electrodes, and therefore have not been quantitatively investigated. In our study, since HIFU ablation was performed without tissue contact, the OAP baseline drift was most likely introduced by HIFU generated temperature changes (Fig. 2). Using high-resolution IR thermography and optical mapping, we quantitatively correlated the OAP baseline drift with temperature for the first time. Since the observed increase in OAP baseline corresponds to a decrease in the total fluorescence, we speculate that the reduced fluorescence stems from three sources: (1) thermal response of the dye because the excitation spectrum shift of the VSD is temperature dependent (Clarke and Kane 1997), (2) changes in tissue properties (e.g. membrane fluidity) which can affect dye-membrane binding process, and (3) temperature-induced changes in the resting membrane potentials (RMP) due to HIFU exposure. Nath *et al*. demonstrated that the RMP was sigmoidally correlated with temperature increases (Nath et al. 1993). In our study, the correlation between OAP baseline and temperature during HIFU heating was linear (Figs. 2D – E), suggesting the RMP increases were not the only cause of the OAP baseline drift. Jin *et al*. observed that the fluorescence of a similar di-4-ANEP dye can be affected by the membrane status, which became liquid-disordered above a transition temperature and solid phase below that temperature (Jin et al. 2006). In our experiments, the membrane phospholipids of the myocytes may become more fluid-like when the temperature crossed certain threshold, and caused the baseline fluorescence drift. Overall, the three mechanisms could all contribute to the drift of OAP baseline and cannot be studied in isolation under our current setup. Determining the exact mechanisms causing the fluorescence baseline shift can help us better interpret the measured fluorescence signals of optical mapping and exclude other confounding factors such as electrical effect.

EP Characteristics Correlated with Temperature and Thermal Dose

Significant EP changes including APA reduction, APD shortening, and increases of conduction time have been observed previously in hyperthermia, RF, and microwave ablation (Nath et al. 1993; Whayne et al. 1994; Wood and Fuller 2002). In this study, we observed similar EP responses induced by HIFU ablation with more spatiotemporal details, and the dynamics of EP changes were quantitatively investigated and correlated with 2D temperature and thermal dose for the first time. While our results are generally consistent with previous studies, several new findings are noted due to the advancements of the IR thermography and optical mapping technologies.

Reduction of APA was previously observed to be linearly dependent on temperature between 37.0 °C and 49.9 °C with a low coefficient of determination (Pearson's r value = 0.54) (Nath et al. 1993). Alternatively, our results showed that APA decreased nonlinearly

with HIFU induced temperature rises (Fig. 7A), with $\Delta APA/\Delta T$ being increasing during HIFU application. The nonlinearity was more apparent between ΔAPA and thermal dose ($\log_{10}(CEM_{43})$). A significant APA reduction occurred at the temperature threshold around 42 °C on the ΔAPA-*T* curve (Fig. 7A) and at thermal dose threshold around −5 on the $\Delta APA/\log_{10}(CEM_{43})$ curve (Fig. 7C), where APA reduced by only 5% below the thresholds but reduced by greater than 25% when above the thresholds. Using ROC analysis, we calculated the temperature threshold for generating significant APA changes to be ≥ 42.7 ± 0.1 °C, consistent with earlier results (42.7 °C ~ 51.8 °C) (Nath et al. 1993). For the first time, the thermal dose threshold ($\log_{10}(CEM_{43})$) for causing significant APA changes was calculated to be greater than −5.30 ± 0.13. Since APA changes are predominantly affected by the kinetics of sodium ion channels, the slight APA reduction at the early stage is likely due to the changes in diffusion rate of sodium upon HIFU induced temperature increases, whereas multiple effects including rises of RMP, blocking of fast sodium channels (Wu et al. 2013), and structural changes of cellular membrane (Jin et al. 2006) were potentially involved when temperature was further increased by HIFU and drastic APA reduction occurred.

Shortening of APD was previously observed to be linearly dependent on temperature for hyperthermia (Pearson's $r < 0.5$) (Nath et al. 1993). Wu *et al*. reported a nonlinear reduction of APD_{80} during RF ablation with significant $\Delta APD_{80}/T$ changes at the beginning of RF application and slight $\Delta APD_{80}/T$ changes later. The damaging and recovering phases of APD_{80} followed a counterclockwise hysteretic loop on the ΔAPD_{80}–*T* curve and they discovered that such hysteresis behavior suggested a combined electrotonic and thermal effects for RF ablation (Wu et al. 1999). In our study, however, the ΔAPD_{50}–*T* curve appeared to be more linear throughout HIFU application, and the relationship was similar to the results using a direct heating element by Wu *et al.*, indicating that HIFU ablation was primarily thermal mediated and the likelihood of interferences from ultrasound radiation force and cavitation was small. Instead of a counterclockwise hysteresis, a clockwise damaging-recovery hysteretic sequence during and after HIFU application (Fig. 7B) was seen in our study. Ideally when no tissue injury was generated, the ΔAPD_{50}–*T* curve during heating and cooling periods should be overlapping or parallel. However, Fig. 7B suggested that the temperature cooling outpaced the recovery of APD_{50} after HIFU application (left pointed arrows), resulting in a separation between damaging and recovering curves. The non-parallel separation between heating and cooling suggested that EP properties and cell functions were transiently impaired by HIFU as the peak temperature approached 50 °C. Such transient injuries may have led to a slower post-HIFU APD_{50} recovery and caused the phenotyping clockwise hysteresis. Moreover, the separation between heating and cooling periods was large for irreversible (ID) cases whereas small for reversible (RD) cases, providing a potential assessment of the degree of tissue injury.

Another important finding was that the region with ΔAPD_{50} extended far beyond the HIFU focus while the region with ΔAPA was more confined surrounding the focus (Fig. 3 and Fig. 5), suggesting a higher thermal sensitivity for APD_{50} and a higher thermo-tolerance for APA. As discussed earlier, the reduction of APA and thermal thresholding effects on APA could be a combined effects of changing in RMP, inactivation of fast sodium channels, and

membrane fluidity, while the shortening of APD and early diminishment of plateau phase is most likely due to the unbalanced calcium and potassium channel kinetics. Calcium channel blockers such as nisoldipine were previously shown to be capable of shortening the effective refractory period (ERP) or APD (Azhari 2010), we therefore hypothesize that HIFU induced temperature increases may have impaired both Ca^{2+} and K^{+} channels and cause the excessive potassium efflux against calcium influx, leading to the shortened APD_{50}. This assumption can be confirmed by the work of Puglisi *et al.*, who demonstrated temperature increases from 25 °C to 35 °C can cause rapid inactivation of L-type calcium channels and abbreviate the APD (Puglisi et al. 1999). In the current study, we also found the temperature threshold for generating significant APD_{50} change to be ≥ 39.6 ± 0.1°C (ROC AUC = 0.67 ± 0.06), which was greatly lower than the temperature threshold for causing APA changes (42.7 ± 0.1 °C, $p < 0.05$) (Fig. 8 and Fig. 9, Table 1). This suggests that a lower temperature threshold may exist for deactivating Ca^{2+} and K^{+} channels as compared to affecting Na^{+} channels. However, further validations using absolute EP measurements are needed to confirm our hypothesis.

Previous studies of HIFU cardiac ablation primarily focused on the correlations between acoustic parameters (i.e. acoustic intensity, duty cycle, and pulse-repetition-frequency) and tissue necrosis alone (Engel et al. 2006; Okumura et al. 2008; Villamizar et al. 2010). A temperature of ≥ 50 °C is often used to ensure permanent tissue physical damage. Another lesion assessment metric, the thermal dose, is also employed and calculated as the cumulative equivalent minutes at 43 °C (CEM_{43}) which captures the time history of temperature changes or total thermal energy deposition. In a recent study using infrared thermography, our group directly attained the critical value of CEM_{43} for generating permanent tissue necrosis to be 170 min under HIFU ablation in *ex vivo* porcine myocardium (Zhou et al. 2006). Along with tissue necrosis, EP characteristics is critically important for HIFU ablation in treating cardiac arrhythmias. Temperature criterions corresponding to EP changes may provide information that are more relevant for devising strategies to optimize HIFU ablation to avoid recurrence of conduction in atrial fibrillation therapy (Laughner et al. 2012b; Oral et al. 2002). In general, thermal dose, as the accumulative effects of temperature may provide a better metric for evaluating thermal ablation outcome. For our specific experiments, the correlation of temperature and thermal dose with EP changes are similar during HIFU ablation (Fig. 7). In this study, using simultaneous IR-EP mapping system, we categorized the HIFU ablation outcomes into reversible and irreversible groups by considering both tissue physical and EP changes including APA and APD, and obtained the lethal isotherm of temperature to be above 52.3 ± 1.4 °C (n = 5), in closer agreement with previous results using RF (Nath et al. 1993; Whayne et al. 1994), and thermal dose ($\log_{10}(CEM_{43})$) isotherm to be above 2.16 ± 0.51 (n = 5). We also found that the EP changes, especially activation pattern and conduction velocities (Figs. 4A1 – C1), could be transiently reformed for up to 30 s but still be reversible when HIFU induced temperature was 50.1 ± 0.8 °C. This provides an opportunity of using HIFU as a pre-ablation testing metric (similar to cryomapping used in clinical (Liu et al. 2006)) to pinpoint the desired ablation sites and temporarily change the tissue conduction prior to permanent ablation. However, Figs. 4A2 – C2 did not show complete electrical conduction block for irreversible cases, and the reasons for such non-sustained conduction block

included optical photon “bleed-over” from adjacent pixels, and AP propagation surrounding and through the gaps of the non-transmural lesions.

Using 2D IR-EP imaging, we observed radially decreased distributions of temperature, APA, and APD around the coagulated tissue (Fig. 8), similar to RF and microwave ablation (Whayne et al. 1994; Wu et al. 1999). HIFU ablated areas were further categorized into three zones: *lesion*, *transition* and *remote* zones, based on tissue physical and EP changes, and different histological changes within each zone were identified. However, within the transition zone, we only observed a narrow band of inflammations (50 – 70 μm) using MT staining while Nath *et al.* observed damages of plasma membrane, mitochondria, gap junctions, and microvasculatures as well as reduction of blood flow surrounding the RF lesion using electron microscopy (Nath et al. 1994a; Nath et al. 1994b). It is important to know that tissue within the lesion peripheral will experience either apoptosis or self-healing, which may explain some of the delayed conduction blocks or recurrence of conduction observed in clinical (Ouyang et al. 2005). Wood *et al.* further elucidated that the acute peri-lesional EP changes induced by RF ablation would eventually resolve in 22 ± 13 days (Wood and Fuller 2002). Therefore, we believe the APA and APD abnormalities within the transition zone observed in our study were likely to recover in a long term.

Perfusion-related Heat Loss during HIFU Ablation

The “heat sink” effect due to major blood vessel has been documented for RF ablation. Especially for ablation at the mitral isthmus (MI), 42 % patients showed unsuccessful MI block when ablation was performed close to a coronary artery (Kurotobi et al. 2011). HIFU induced heating can also be conducted away by blood perfusion in treating liver tumors, thereby more HIFU energy was needed to achieve desired ablation volume (Jiang et al. 2013). The efficacy of HIFU ablation close to blood vessels may depend on the diameter of the vessel and the flow rate of the blood perfusion. Using IR thermography, we directly observed heat loss by coronary artery flow and the resultant asymmetric lesion geometry during HIFU cardiac ablation (Fig. 10). However, no significant EP damage along the LAD coronary artery was generated by HIFU. Perivascular viable tissue was obtained pathologically and may help explain the effect associated with incomplete lesion line in HIFU ablation (Laughner et al. 2012b) and recurrence of AF in clinical settings (Kurotobi et al. 2011). Geometric narrowing of lesion towards the epicardium was observed for most HIFU lesions, which can be the result of arterial flow and superfusion.

Limitations

A Langendorff-perfused rabbit heart model was used in this study, thus results may vary for other species and differ from *in vivo* condition. The excitation-contraction decoupler (BDM) may affect the normal ion channel properties. In addition, continuous light illumination can weaken BDM and cause photo bleaching of the VSD, affecting the accuracy of the OAP measurement. Although we corrected photobleaching using curve fittings, a dual-wavelength ratiometric method may be more precise. Finally, both optical mapping and IR imaging are technically limited to epicardial measurements due to light absorption across tissue thickness.

Conclusions

HIFU ablation generates cardiac tissue changes accompanied by changes in myocardial EP with different spatiotemporal characteristics, including reversible and irreversible reduction of APA, shortening of APD_{50}, delayed activation, and distortions of activation patterns. Temperature and thermal dose criterions can provide important information regarding reversible and irreversible tissue and EP changes. APD_{50} was found to be more thermally sensitive than APA, suggesting cardiac AP plateau potentials were more thermal vulnerable than cellular excitabilities. Isotherms of temperature and corresponding thermal doses were determined for generating lesion, APA changes, and APD shortening. Major vessels related to the "heat sink" effect can also compromise the efficacy of HIFU ablation. These results may provide guidance to ensure persistent and meaningful EP changes and conduction block desired for clinical HIFU cardiac ablation procedures.

Acknowledgments

This work was supported by funding from NIH (R01 EP008999) and the University of Michigan. The authors acknowledge technical assistance from K. Ives, Y. Zhou, YS. Hsiao, M.S.R. Gudur, TY. Wang, KW. Lin, Y. Kim, B. Okura, and K. Morrison.

References

Aktas MK, Daubert JP, Hall B. Surgical atrial fibrillation ablation: a review of contemporary techniques and energy sources. Cardiol J. 2008; 15(1):87–94. [PubMed: 18651392]

Azhari, H. Basics of Biomedical Ultrasound for Engineers. Hoboken, NJ, USA: John Wiley & Sons, Inc; 2010. Appendix A: Typical Acoustic Properties of Tissues.

Clarke RJ, Kane DJ. Optical detection of membrane dipole potential: avoidance of fluidity and dye-induced effects. Biochim Biophys Acta. 1997; 1323(2):223–239. [PubMed: 9042345]

Deng CX, Qu F, Nikolski VP, Zhou Y, Efimov IR. Fluorescence imaging for real-time monitoring of high-intensity focused ultrasound cardiac ablation. Ann Biomed Eng. 2005; 33(10):1352–1359. [PubMed: 16240084]

Dewire J, Calkins H. State-of-the-art and emerging technologies for atrial fibrillation ablation. Nat Rev Cardiol. 2010; 7(3):129–138. [PubMed: 20179720]

Engel DJ, Muratore R, Hirata K, Otsuka R, Fujikura K, Sugioka K, Marboe C, Lizzi FL, Homma S. Myocardial lesion formation using high-intensity focused ultrasound. J Am Soc Echocardiogr. 2006; 19(7):932–937. [PubMed: 16825005]

Fishbein MC, Meerbaum S, Rit J, Lando U, Kanmatsuse K, Mercier JC, Corday E, Ganz W. Early phase acute myocardial infarct size quantification: validation of the triphenyl tetrazolium chloride tissue enzyme staining technique. Am Heart J. 1981; 101(5):593–600. [PubMed: 6164281]

Fujikura K, Otsuka R, Kalisz A, Ketterling JA, Jin Z, Sciacca RR, Marboe CC, Wang J, Muratore R, Feleppa EJ, Homma S. Effects of ultrasonic exposure parameters on myocardial lesions induced by high-intensity focused ultrasound. J Ultrasound Med. 2006; 25(11):1375–1386. [PubMed: 17060423]

Fuller IA, Wood MA. Intramural coronary vasculature prevents transmural radiofrequency lesion formation: implications for linear ablation. Circulation. 2003; 107(13):1797–1803. [PubMed: 12665492]

Giridhar D, Robinson RA, Liu Y, Sliwa J, Zderic V, Myers MR. Quantitative estimation of ultrasound beam intensities using infrared thermography-Experimental validation. J Acoust Soc Am. 2012; 131(6):4283–4291. [PubMed: 22712903]

Haines DE. The biophysics of radiofrequency catheter ablation in the heart: the importance of temperature monitoring. Pacing Clin Electrophysiol. 1993; 16(3 Pt 2):586–591. [PubMed: 7681962]

Jiang F, He M, Liu YJ, Wang ZB, Zhang L, Bai J. High intensity focused ultrasound ablation of goat liver in vivo: Pathologic changes of portal vein and the “heat-sink” effect. Ultrasonics. 2013; 53(1):77–83. [PubMed: 22583752]

Jin L, Millard AC, Wuskell JP, Dong X, Wu D, Clark HA, Loew LM. Characterization and application of a new optical probe for membrane lipid domains. Biophys J. 2006; 90(7):2563–2575. [PubMed: 16415047]

Kannel WB, Cupples LA, D’Agostino RB. Sudden death risk in overt coronary heart disease: the Framingham Study. Am Heart J. 1987; 113(3):799–804. [PubMed: 3825868]

Khokhlova VA, Shmeleva SM, Gavrilov LR, Martin E, Sadhoo N, Shaw A. Infrared mapping of ultrasound fields generated by medical transducers: feasibility of determining absolute intensity levels. J Acoust Soc Am. 2013; 134(2):1586–1597. [PubMed: 23927199]

Knisley SB. Transmembrane voltage changes during unipolar stimulation of rabbit ventricle. Circ Res. 1995; 77(6):1229–1239. [PubMed: 7586236]

Kurotobi T, Shimada Y, Kino N, Iwakura K, Inoue K, Kimura R, Tosyoshima Y, Mizuno H, Okuyama Y, Fujii K, Nanto S, Komuro I. Local coronary flow is associated with an unsuccessful complete block line at the mitral isthmus in patients with atrial fibrillation. Circ Arrhythm Electrophysiol. 2011; 4(6):838–843. [PubMed: 21984444]

Lall SC, Damiano RJ Jr. Surgical ablation devices for atrial fibrillation. J Interv Card Electrophysiol. 2007; 20(3):73–82. [PubMed: 18175210]

Laughner JI, Ng FS, Sulkin MS, Arthur RM, Efimov IR. Processing and analysis of cardiac optical mapping data obtained with potentiometric dyes. Am J Physiol Heart Circ Physiol. 2012a; 303(7):H753–765. [PubMed: 22821993]

Laughner JI, Sulkin MS, Wu Z, Deng CX, Efimov IR. Three potential mechanisms for failure of high intensity focused ultrasound ablation in cardiac tissue. Circ Arrhythm Electrophysiol. 2012b; 5(2): 409–416. [PubMed: 22322367]

Liu Y, Kon T, Li C, Zhong P. High intensity focused ultrasound-induced gene activation in solid tumors. J Acoust Soc Am. 2006; 120(1):492–501. [PubMed: 16875245]

Loew LM. Voltage-sensitive dyes: measurement of membrane potentials induced by DC and AC electric fields. Bioelectromagnetics. 1992; (Suppl 1):179–189. [PubMed: 1285714]

Madding, RP. Emissivity measurement and temperature correction accuracy considerations. In: LeMieux, DH.; Snell, JR., Jr, editors. SPIE. Orlando, FL, USA: SPIE; p. 393-401.

Metzner A, Chun KR, Neven K, Fuernkranz A, Ouyang F, Antz M, Tilz R, Zerm T, Koektuerk B, Wissner E, Koester I, Ernst S, Boczor S, Kuck KH, Schmidt B. Long-term clinical outcome following pulmonary vein isolation with high-intensity focused ultrasound balloon catheters in patients with paroxysmal atrial fibrillation. Europace. 2010; 12(2):188–193. [PubMed: 20089752]

Nanthakumar K, Plumb VJ, Epstein AE, Veenhuyzen GD, Link D, Kay GN. Resumption of electrical conduction in previously isolated pulmonary veins: rationale for a different strategy? Circulation. 2004; 109(10):1226–1229. [PubMed: 14993124]

Nath S, Lynch C 3rd, Whayne JG, Haines DE. Cellular electrophysiological effects of hyperthermia on isolated guinea pig papillary muscle. Implications for catheter ablation. Circulation. 1993; 88(4 Pt 1):1826–1831. [PubMed: 8403328]

Nath S, Redick JA, Whayne JG, Haines DE. Ultrastructural observations in the myocardium beyond the region of acute coagulation necrosis following radiofrequency catheter ablation. J Cardiovasc Electrophysiol. 1994a; 5(10):838–845. [PubMed: 7874329]

Nath S, Whayne JG, Kaul S, Goodman NC, Jayaweera AR, Haines DE. Effects of radiofrequency catheter ablation on regional myocardial blood flow. Possible mechanism for late electrophysiological outcome. Circulation. 1994b; 89(6):2667–2672. [PubMed: 8205679]

Neven K, Schmidt B, Metzner A, Otomo K, Nuyens D, De Potter T, Chun KR, Ouyang F, Kuck KH. Fatal end of a safety algorithm for pulmonary vein isolation with use of high-intensity focused ultrasound. Circ Arrhythm Electrophysiol. 2010; 3(3):260–265. [PubMed: 20504943]

Ninet J, Roques X, Seitelberger R, Deville C, Pomar JL, Robin J, Jegaden O, Wellens F, Wolner E, Vedrinne C, Gottardi R, Orrit J, Billes MA, Hoffmann DA, Cox JL, Champsaur GL. Surgical ablation of atrial fibrillation with off-pump, epicardial, high-intensity focused ultrasound: results of a multicenter trial. J Thorac Cardiovasc Surg. 2005; 130(3):803–809. [PubMed: 16153932]

Okumura Y, Kolasa MW, Johnson SB, Bunch TJ, Henz BD, O'Brien CJ, Miller DV, Packer DL. Mechanism of tissue heating during high intensity focused ultrasound pulmonary vein isolation: implications for atrial fibrillation ablation efficacy and phrenic nerve protection. J Cardiovasc Electrophysiol. 2008; 19(9):945–951. [PubMed: 18399966]

Oral H, Knight BP, Ozaydin M, Tada H, Chugh A, Hassan S, Scharf C, Lai SW, Greenstein R, Pelosi F Jr, Strickberger SA, Morady F. Clinical significance of early recurrences of atrial fibrillation after pulmonary vein isolation. J Am Coll Cardiol. 2002; 40(1):100–104. [PubMed: 12103262]

Ouyang F, Antz M, Ernst S, Hachiya H, Mavrakis H, Deger FT, Schaumann A, Chun J, Falk P, Hennig D, Liu X, Bansch D, Kuck KH. Recovered pulmonary vein conduction as a dominant factor for recurrent atrial tachyarrhythmias after complete circular isolation of the pulmonary veins: lessons from double Lasso technique. Circulation. 2005; 111(2):127–135. [PubMed: 15623542]

Parsons JE, Cain CA, Fowlkes JB. Cost-effective assembly of a basic fiber-optic hydrophone for measurement of high-amplitude therapeutic ultrasound fields. J Acoust Soc Am. 2006; 119(3): 1432–1440. [PubMed: 16583887]

Puglisi JL, Yuan W, Bassani JW, Bers DM. Ca(2+) influx through Ca(2+) channels in rabbit ventricular myocytes during action potential clamp: influence of temperature. Circ Res. 1999; 85(6):e7–e16. [PubMed: 10488061]

Rivens I, Shaw A, Civale J, Morris H. Treatment monitoring and thermometry for therapeutic focused ultrasound. Int J Hyperthermia. 2007; 23(2):121–139. [PubMed: 17578337]

Sapareto SA, Dewey WC. Thermal dose determination in cancer therapy. Int J Radiat Oncol Biol Phys. 1984; 10(6):787–800. [PubMed: 6547421]

Scheinman MM, Morady F. Nonpharmacological approaches to atrial fibrillation. Circulation. 2001; 103(16):2120–2125. [PubMed: 11319205]

Strickberger SA, Tokano T, Kluiwstra JU, Morady F, Cain C. Extracardiac ablation of the canine atrioventricular junction by use of high-intensity focused ultrasound. Circulation. 1999; 100(2): 203–208. [PubMed: 10402451]

Villamizar NR, Crow JH, Piacentino V 3rd, DiBernardo LR, Daneshmand MA, Bowles DE, Groh MA, Milano CA. Reproducibility of left atrial ablation with high-intensity focused ultrasound energy in a calf model. J Thorac Cardiovasc Surg. 2010; 140(6):1381–1387. [PubMed: 20934725]

Whayne JG, Nath S, Haines DE. Microwave catheter ablation of myocardium in vitro. Assessment of the characteristics of tissue heating and injury. Circulation. 1994; 89(5):2390–2395. [PubMed: 8181165]

Wood MA, Fuller IA. Acute and chronic electrophysiologic changes surrounding radiofrequency lesions. J Cardiovasc Electrophysiol. 2002; 13(1):56–61. [PubMed: 11843484]

Wu CC, Fasciano RW 2nd, Calkins H, Tung L. Sequential change in action potential of rabbit epicardium during and following radiofrequency ablation. J Cardiovasc Electrophysiol. 1999; 10(9):1252–1261. [PubMed: 10517659]

Wu Z, Gudur MS, Deng CX. Transmural ultrasound imaging of thermal lesion and action potential changes in perfused canine cardiac wedge preparations by high intensity focused ultrasound ablation. PloS one. 2013; 8(12):e82689. [PubMed: 24349337]

Zhou Y, Zhai L, Simmons R, Zhong P. Measurement of high intensity focused ultrasound fields by a fiber optic probe hydrophone. J Acoust Soc Am. 2006; 120(2):676–685. [PubMed: 16938956]

Zimmer JE, Hynynen K, He DS, Marcus F. The feasibility of using ultrasound for cardiac ablation. IEEE Trans Biomed Eng. 1995; 42(9):891–897. [PubMed: 7558063]

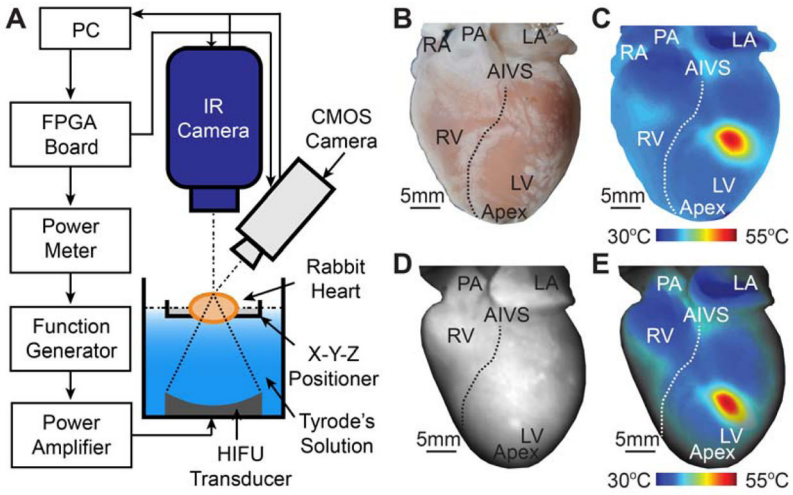

Figure 1. Experimental setup and image registration

(A) Schematic diagram: infrared (IR) camera for temperature imaging and high-speed fluorescence CMOS camera for optical mapping of electrophysiology are confocally aligned focusing at the upper epicardium of the rabbit heart preparation. The HIFU transducer at the bottom of the tissue chamber is facing upwards with its focus at the upper myocardium within the field-of-view of the two cameras. The heart is mostly submersed in the perfusion and superfusion system with only portion of the upper epicardium above the solution to permit IR imaging. (B) Photograph of a rabbit heart preparation. (C) Corresponding infrared (IR) image during HIFU ablation (t = 14 s). (D) Background image of optical mapping. (E) Overlaid image of projective transformed IR and optical mapping image based on physical landmarks (e.g. atrial-ventricular groove). RA = Right Atrium; LA = Left Atrium; RV = Right Ventricle; LV = Left Ventricle; AIVS = Anterior Inter-Ventricular Sulcus.

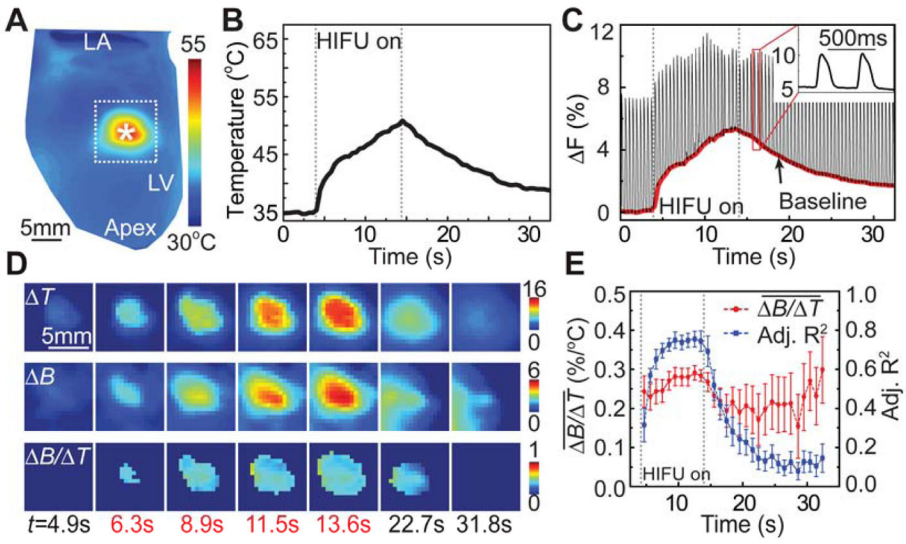

Figure 2. Changes of optical action potentials (OAPs) baseline and temperature, and their correlation

(A) Temperature map from infrared (IR) imaging at t = 14.5 s. (B) A representative temperature trace at asterisk labeled location within HIFU focus in (A) with maximum temperature rise in the region-of-interest (ROI). (C) Corresponding OAPs trace at the same location in (A) with each "spikes" corresponding to single cardiac cycle. The bold line highlights the baseline of fractional fluorescence signal (Δ*F*). HIFU was on from 4 s to 14 s (shaded area). The inset shows an enlarged version of two OAPs. (D) Maps of temperature changes (Δ*T*) and corresponding OAP baseline changes (Δ*B*) in the ROI in white dashed box in (A). Ratiometric map of Δ*B*/Δ*T* at corresponding times (bottom). HIFU was applied from 4 s to 14 s. (E) Linear regression slope ($\overline{\Delta B/\Delta T}$) for paired Δ*B*–Δ*T* frames and adjusted R^2 as function of time (n = 7). HIFU is applied *in situ* during the shaded period.

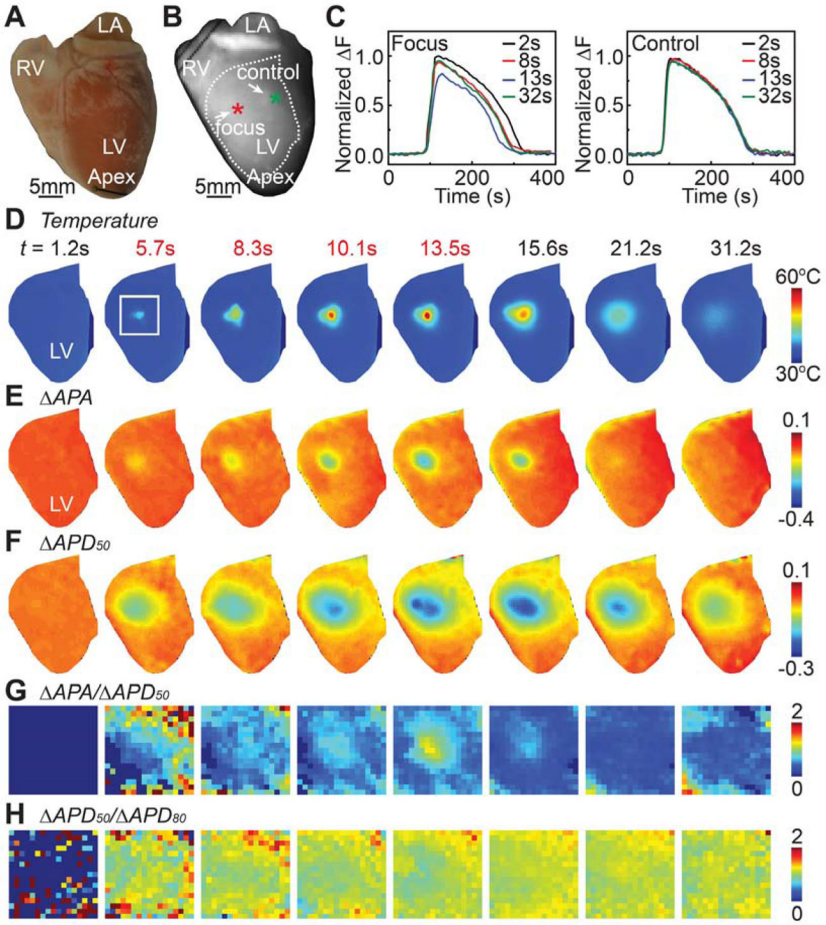

Figure 3. Example of a reversible ablation case

(A) Photograph of a gross rabbit heart. (B) Background image of optical mapping of the same heart with region-of-interest (ROI) encircled by the dashed line. (C) Superimposed normalized single OAPs in the HIFU focus and outside in the control region at asterisks labeled location in (B) at t = 2 s, 8 s, 13 s, and 32 s. (D) Temperature maps in the ROI displayed in (B) at indicated time with HIFU application on from 4 s to 14 s. (E) Maps of APA changes (ΔAPA) in the same ROI. (F) Maps of APD_{50} changes (ΔAPD_{50}). (G) Maps of $\Delta APA/\Delta APD_{50}$ in the smaller ROI of box in (D). (H) Maps of $\Delta APD_{50}/\Delta APD_{80}$ in the same ROI.

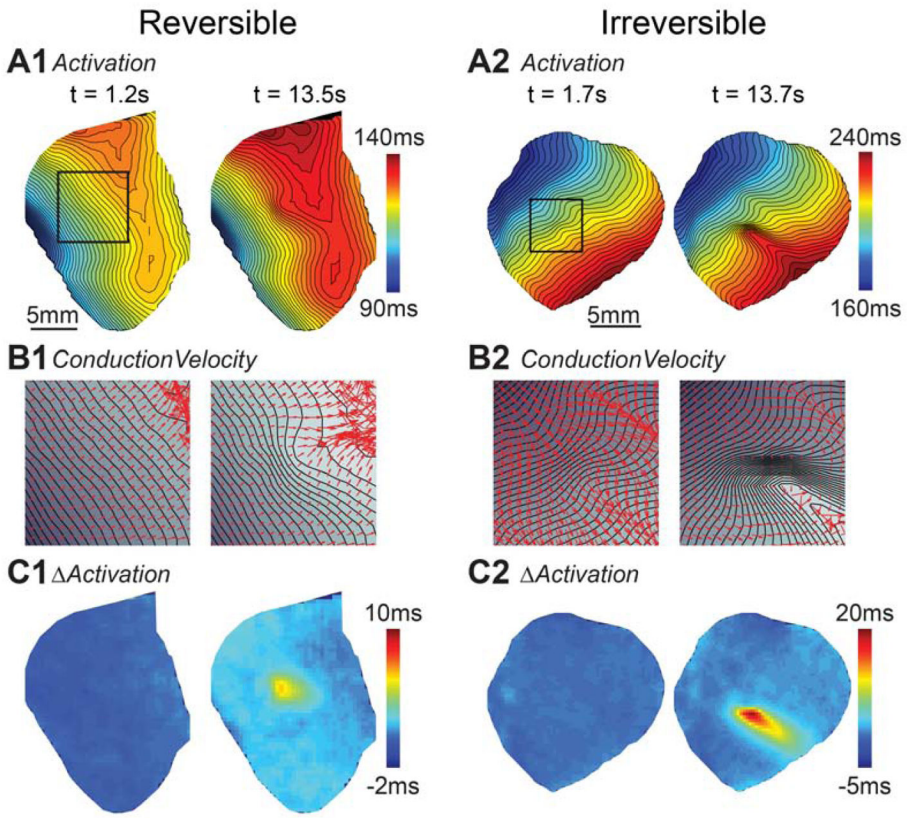

Figure 4. Activation changes for reversible and irreversible cases

(A) Activation map prior, during, and post HIFU ablation for reversible damage (A1, RD) at t = 1.2 s and 13.5 s, and for irreversible damage (A2, ID) at t = 1.7 s and 13.7 s. Isochrones are separated at 1 ms step size. (B) Maps of conduction velocity (CV) within the box labeled smaller ROI in (A) for RD (B1) and ID (B2). Arrows point the direction of electrical conduction and their lengths represent corresponding magnitudes of CV. (C) Maps of activation delay derived by subtracting activation maps from their pre-HIFU state for RD (C1) and ID (C2).

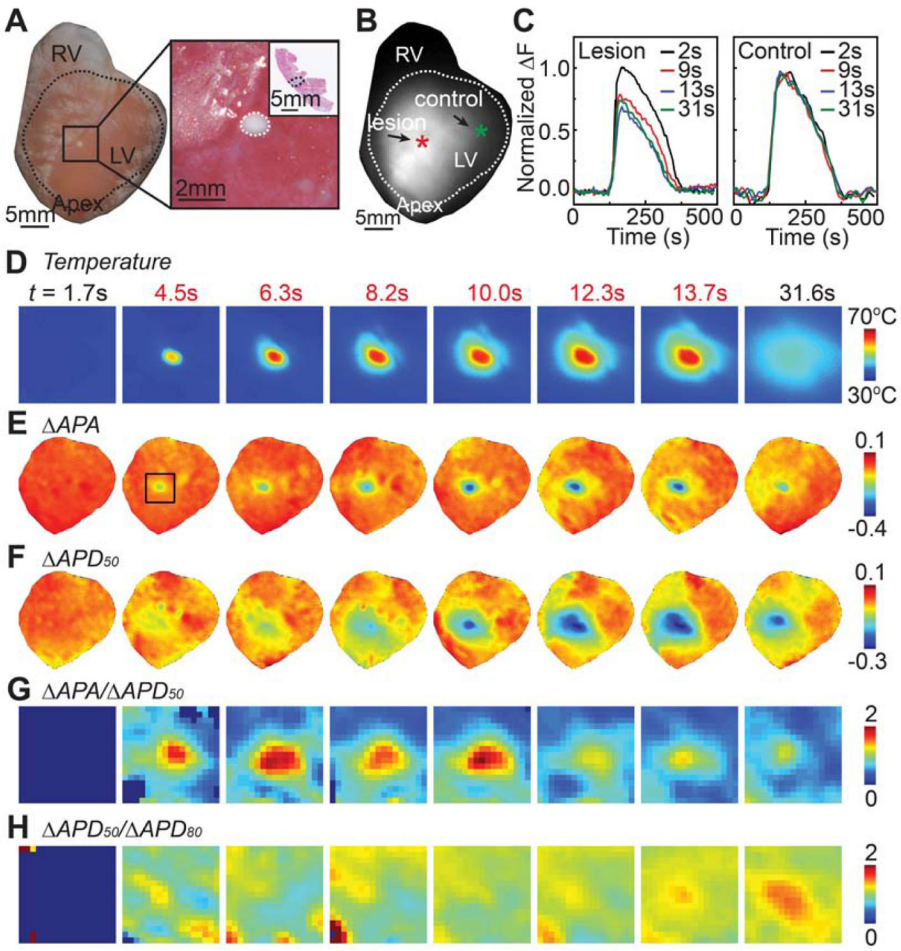

Figure 5. Example of an irreversible ablation case

(A) Photograph of gross heart with region-of-interest (ROI) encircled by the dash line. The enlarged area in the box shows TTC stained tissue specimen with lesion in the middle (dashed line). The inset shows a tissue cross-section stained with Masson's trichrome with lesion indicated by the dashed line. (B) Background image of optical mapping of the same heart with the same ROI in (A) encircled by the dash line. (C) Superimposed normalized single OAPs in the HIFU lesion and outside in the control region at the asterisks labeled locations in (B) at t = 2 s, 9 s, 13s, and 31 s. (D) Temperature maps in the smaller ROI in (A, box region) at indicated time with HIFU on from 4 s to 14 s. (E) Maps of APA changes (ΔAPA) in the large ROI displayed in (A). (F) Maps of APD_{50} changes (ΔAPD_{50}) in the same ROI. (G) Maps of $\Delta APA/\Delta APD_{50}$ in the smaller ROI of the box in (E). (H) Maps of $\Delta APD_{50}/\Delta APD_{80}$ in the same ROI.

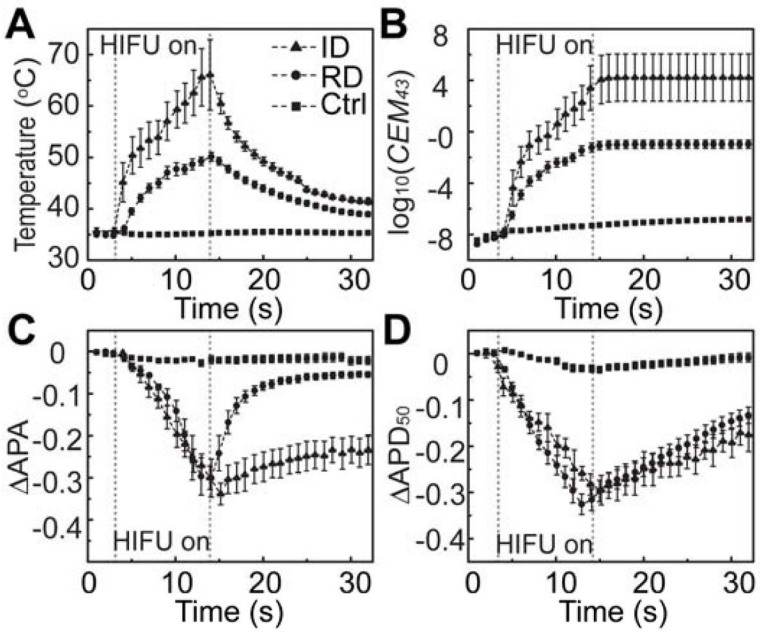

Figure 6. Temporal traces of temperature and EP parameters

Statistical progression of (A) temperature, (B) logarithmic CEM_{43} ($\log_{10}(CEM_{43})$), (C) ΔAPA, and (D) ΔAPD_{50} for reversible damage (RD) and irreversible damage (ID) in the center of HIFU focus as well as control (Ctrl, normal tissue). Plots are presented as mean ± SEM. HIFU was on from 4 s to 14 s.

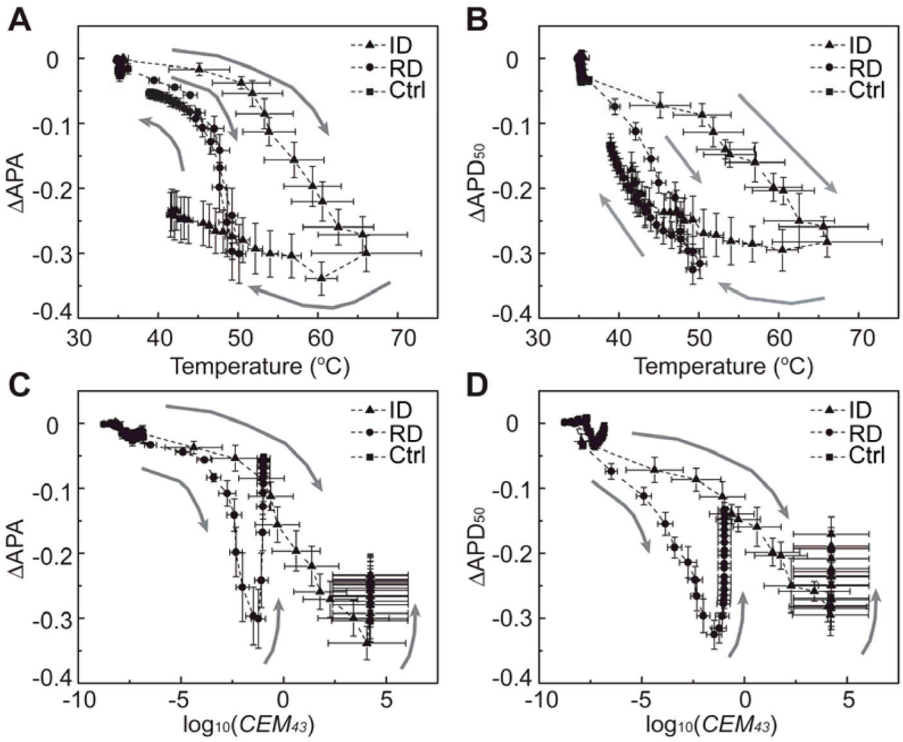

Figure 7. Correlation between EP parameters and temperature

(A) ΔAPA vs. temperature, (B) ΔAPD_{50} vs. temperature, (C) ΔAPA vs. $\log_{10}(CEM_{43})$, and (D) ΔAPD_{50} vs. $\log_{10}(CEM_{43})$ for RD, ID, and Ctrl (control) during and after HIFU application. Arrows indicate the direction of the temporal trends (damaging and recovery) for each parameter. Data are presented as mean ± SEM.

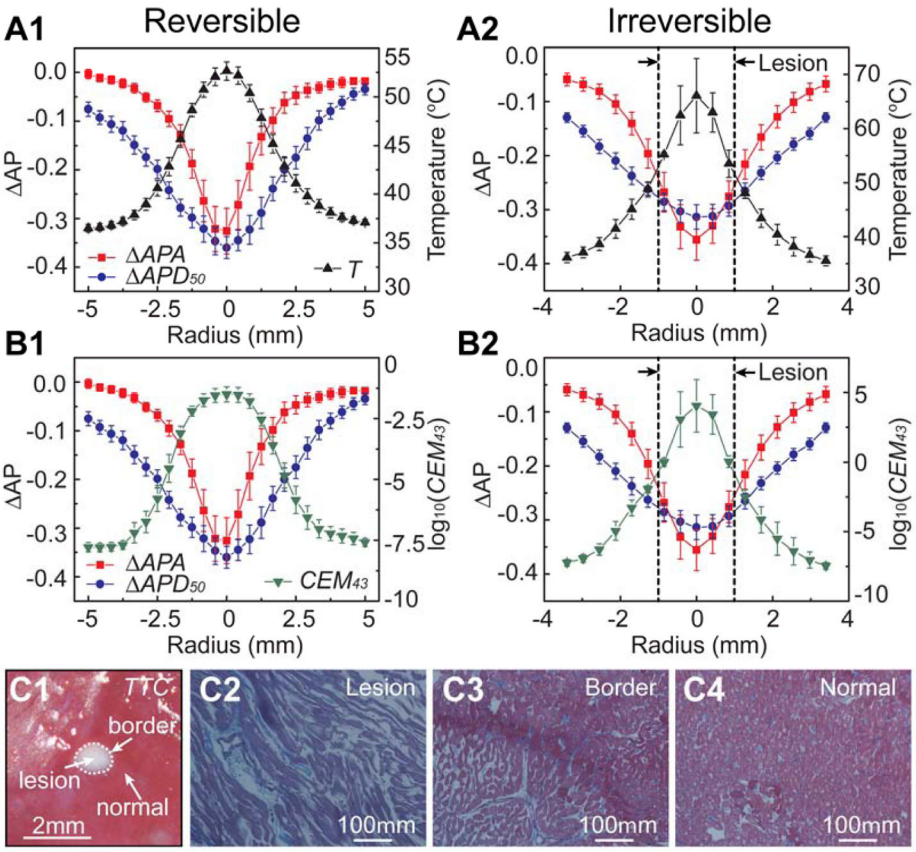

Figure 8. Spatial characteristics of lesion and AP changes

(A) Radial profiles of ΔAPA, ΔAPD_{50}, and temperature for reversible (A1, $n = 9$) and irreversible (A2, $n = 5$) cases. (B) Radial profiles of ΔAPA, ΔAPD_{50}, and $\log_{10}(CEM_{43})$ for reversible (B1) and irreversible (B2) cases. Lesion region is indicated by double arrows. Reversible cases are on the left column and irreversible cases are on the right. (C1) An example of TTC stained lesion with lesion edge encircled by dashed line. (C2) Masson's trichrome (MT) stained slide (20 X) within lesion. (C3) MT slide of lesion border. (C4) MT slide of normal tissue outside lesion. (C2 – C4) are MT slides for the lesion in (C1).

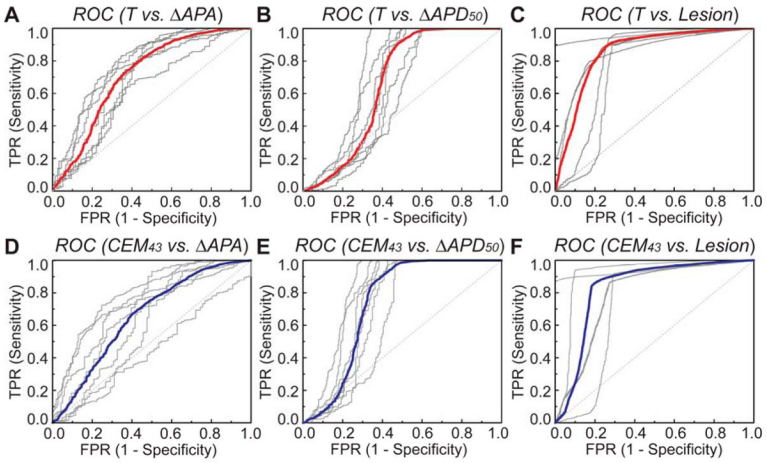

Figure 9. Receiver operating characteristic (ROC) analysis of determining isotherms of temperature and thermal doses for APA, APD_{50}, and Lesion

Individual ROC curves (thin) and averaged ROC curve (bold) of temperature isotherms for predicting (A) ΔAPA < −0.1, (B) ΔAPD50 < −0.12, and (C) lesion. ROC curves of thermal dose isotherms for predicting (D) ΔAPA < −0.1, (E) ΔAPD50 < −0.12, and (F) lesion.

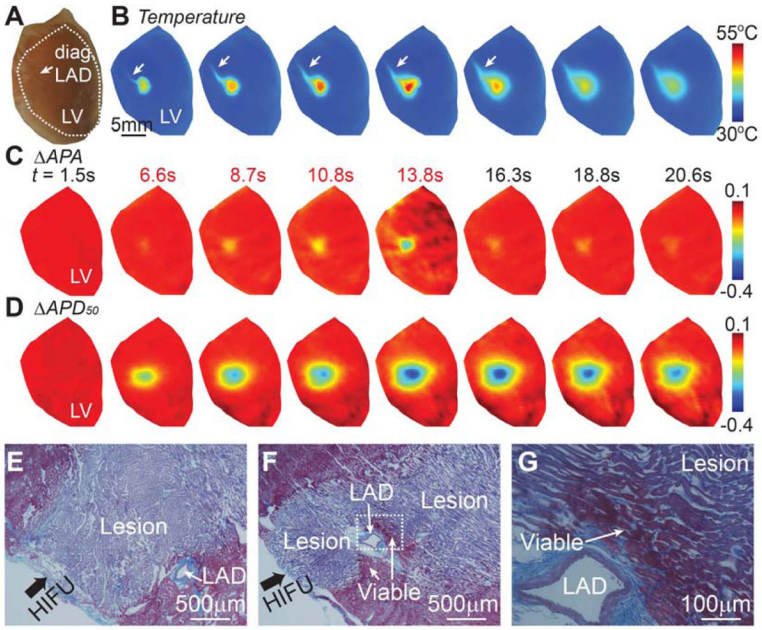

Figure 10. Convective heat loss due to perfusion

(A) Photograph of a gross heart with region-of-interest (ROI) encircled by dashed line. The diagonal branch of a lateral anterior descending (LAD) coronary artery is highlighted by an arrow. (B) IR images during (6.6, 8.7, 10.8, and 13.8 s) and after (16.3, 18.8, and 20.6 s) HIFU ablation with convective heat loss indicated by arrows within the ROI in (A). (C) Corresponding APA changes. (D) Changes of APD_{50}. (E) An example of masson's trichrome (MT) stained lesion with LAD coronary artery aside from the HIFU axial beam. (F) MT slide of a HIFU lesion with LAD coronary artery within the field of HIFU beam. HIFU ablation was applied along the bold arrow direction for both (E) and (F). (G) Magnified image (5X) of ROI of the dashed box in (F). Lesion was stained as dark purple while viable tissue was dark red.

Table 1

Area Under the Curve (AUC) values and thresholds of temperature and thermal dose ($\log_{10}(CEM_{43})$) for generating lesion, APA loss, and APD_{50} loss in HIFU ablation. Results were derived using receiver-operating characteristic (ROC) curve analysis on a pixel-by-pixel basis.

	Temperature		$\log_{10}(CEM_{43})$	
	AUC	**Threshold (°C)**	**AUC**	**Threshold**
Lesion (n = 5)	0.84 ± 0.11	52.3 ± 1.4	0.86 ± 0.12	2.16 ± 0.51
ΔAPA (n = 7)	0.72 ± 0.11	42.7 ± 0.1	0.64 ± 0.16	−5.30 ± 0.13
ΔAPD_{50} (n = 7)	0.67 ± 0.06	39.1 ± 0.1	0.75 ± 0.05	−6.73 ± 0.06